Eur. Phys. J. E (2017) **40**: 20
DOI 10.1140/epje/i2017-11508-6

THE EUROPEAN PHYSICAL JOURNAL E

Regular Article

Shear-induced structural and thermodynamic phase transitions in micellar systems

Angelina Martín del Campo[1], J. Paulo García-Sandoval[1,a], J.F. Armando Soltero[1], Fernando Bautista[1], Octavio Manero[2], and Jorge E. Puig[1]

[1] Departamentos de Ingeniería Química y Física, Universidad de Guadalajara, Blvd. M. García Barragán 1451, Guadalajara, Jal., 44430, Mexico
[2] Instituto de Investigaciones en Materiales, Universidad Nacional Autónoma de México, Ciudad Universitaria, México D. F., 04510, Mexico

Received 4 November 2016 and Received in final form 27 January 2017
Published online: 27 February 2017 –

Abstract. In this contribution a methodology to compute and classify shear-induced structural and phase transitions in surfactant/water mixtures from rheological measurements is presented. Non-linear rheological experiments, considering variations in surfactant concentration and temperature, are analyzed. In particular, the parameters of the BMP (Bautista-Manero-Puig) model, obtained from the fitting of the shear stress *versus* shear rate data, which are functions of surfactant concentration and temperature, allow classifying structural and phase transition boundaries. To test this methodology, we consider the analysis of the shear-induced structural and phase transitions of two micellar systems, cetyltrimethylammonium tosylate (CTAT)/water as a function of CTAT concentrations and Pluronics P103/water as a function of temperature. We found that the CTAT/water system presents a first-order phase transition at 30 °C, and around 31 to 32 wt.% from isotropic to nematic phases, whereas a 20 wt.% Pluronics P103 aqueous micellar solution has two second-order (structural) phase transitions, one from spherical to cylindrical micelles at 33.1 °C, and another one from cylindrical micelles to a nematic phase at 35.8 °C and one first-order phase transition around 37.9 °C at high shear rates near to the cloud point previously reported. The proposed methodology is also able to identify the instability regions where the wormlike micelles are broken, producing the typical shear banding behavior.

1 Introduction

Surfactants in aqueous solutions have the ability to self-aggregate to form micelles. Depending on their concentration [1], first spherical micelles form above the critical micelle concentration (cmc), and upon increasing concentration, flexible wormlike micelles develop [2]. These wormlike micelles have viscoelastic properties similar to those exhibited by polymer solutions and melts, but their rheological behavior is usually more complex because they have the ability to break and restore their structure under flow conditions due to their self-aggregation processes. Hence, an external shear stress causes these giant micelles to continuously extend, interlace, and increase or decrease their size. These processes lead to a reversible shear-induced structural or non-equilibrium phase transitions with spatially inhomogeneous flow patterns named shear bands, resembling the instability between two phases, a highly oriented and non-oriented ones [3]. The shear-induced phase transition (SIPT) mechanism in wormlike micellar solutions is supported by 1) the existence of the plateau stress that is unique, robust and independent of flow history; 2) the long stress oscillations in transient flows that reflect the kinetics of nucleation and growth of a second phase, similar to that observed in equilibrium first-order phase transitions; and 3) the similarities found between the master flow-phase diagram constructed by temperature-concentration superposition and the equilibrium liquid-vapor phase diagrams [4–6]. In this regard, the similarities between the shear-banding transition and a thermodynamic phase transition have been a provocative and standing issue [7–14]. Several models have been proposed to explain shear banding flow, such as the model proposed by Hess [15] for polymeric systems, based on irreversible thermodynamics and a dynamic version of the Landau-de Gennes theory [16], and the Bautista-Manero-Puig (BMP) model for wormlike micellar systems, deduced from the Extended Irreversible Thermodynamics (EIT), which provides an approach to derive hydrodynamic equations governing the behavior of complex fluids [17]. The BMP model includes the coupling of diffusion, stress and the evolution of the structure with

[a] e-mail: paulo.garcia@cucei.udg.mx

time, and has proven to be successful since it predicts well shear thickening followed by shear thinning in dilute micellar solutions [18,19], shear thinning and shear banding flow in semi-dilute and concentrated micellar solutions as well as the homogeneous and the non-homogeneous flow regions, shows the existence of two metastable bands and the long transients and oscillations associated with shear banding flow [6,20]. Moreover, the model is built on solid theoretical background since it was derived using the Irreversible Thermodynamic approach [17,21]. The model has also been used to understand the extensional flow of wormlike micellar solutions. The theory on extensional flows of wormlike micelles using the BMP model was developed by Manero *et al.* [22]. However, and in spite of predicting an increase in the uniaxial extensional viscosity at a critical extension rate, and thereafter an extension-thinning region in accord to experiments, in some regions of the viscosity curve the model becomes unstable. This was also the case in the POM-POM model by McLeish *et al.* [23]. This behavior has been overcome by slight modifications suggested by Boek *et al.* [24] which makes the model stable at all strain rates. An alternative modification can also be suggested by adding a solvent contribution to the original BMP equations. Improvements to the model can also be suggested by modifying the kinetic equation of the structure parameter. This implies alternative expressions to the dissipation term, to account for effects of shear thickening. Moreover, it has been suggested in a recent analysis [25] that this model and others can be improved using a tensorial structure parameter to account for flow reversal experiments in thixotropic fluids.

Thermodynamically, a phase is a system or subsystem with homogeneous chemical composition and physical structure, bounded by a surface along which its properties may change continuously or abruptly. The transition from one configuration to another separated by a boundary (interface) between two states is known as a phase transition. Usually it is given in terms of the profile of some of the thermodynamic parameters of the system near to a critical point [26]. A classification scheme of a phase transition as a function of the system parameters can be suggested: in a first-order phase transition, the molar entropy, molar volume and other parameters undergo discontinuous changes. In addition, there are also transitions of higher order, in which the parameters are continuous, but its derivatives with respect to their conjugate properties are discontinuous [27].

Phase transitions in complex fluids exhibit flow instabilities in regions close to the non-equilibrium critical point. The understanding of these phenomena in complex fluids is an important issue to control the morphology, to predict some of their physicochemical properties and to determine the stability of the system during processing. On this basis, in this work we propose a methodology to identify, classify and locate the shear-induced phase transitions by analyzing the behavior of the BMP model parameters computed from linear and nonlinear rheological experiments, as a function of surfactant concentration and temperature. To test the proposed methodology, we analyze the shear-induced phase transitions in two micellar systems, cetyltrimethylammonium tosylate (CTAT)/water with variations in the CTAT concentrations at constant temperature and Pluronics P103/water with variations in temperature at constant concentration.

2 The BMP model

The BMP (Bautista-Manero-Puig) model is derived from the coupling of the equations of diffusion, stress and the evolution of structure with time [21], and it has been used successfully to reproduce the non-linear behavior of polymer-like micellar solutions and other complex fluids [28]. This model consists of the upper-convected Maxwell equation and a kinetic equation that describes the structure evolution induced by flow. The general form of these equations, where diffusion is neglected, is

$$\underline{\underline{\sigma}} + \lambda_\sigma \overset{\nabla}{\underline{\underline{\sigma}}} = \frac{2}{\varphi}\underline{\underline{D}}, \tag{1}$$

$$\varphi + \lambda \frac{\mathrm{d}\varphi}{\mathrm{d}t} = \varphi_0 + \lambda k \left(II_D\right)\left(\varphi_\infty - \varphi\right)\underline{\underline{\sigma}} : \underline{\underline{D}}. \tag{2}$$

Here $\overset{\nabla}{\underline{\underline{\sigma}}}$ is the upper convected derivative of the stress tensor $\underline{\underline{\sigma}}$, $\underline{\underline{D}}$ is the rate of deformation tensor, φ is the fluidity (or inverse viscosity, $\varphi \equiv \eta^{-1}$), φ_0 and φ_∞ are the fluidities at zero and very high shear rates, respectively, λ is a structural relaxation time, k can be interpreted as a kinetic parameter for structure breaking that depends on the second invariant of the rate of deformation tensor, II_D. Finally, λ_σ (defined as $\lambda_\sigma = (G_0\varphi)^{-1}$, with G_0 as the elastic plateau modulus) is the stress relaxation time that depends on the structural variable of the BMP model. All the parameters of the model can be determined from independent rheological measurements and can be used to predict other flow situations [29]. In general, these parameters are functions of the temperature, T, and surfactant concentration, C. Here it is assumed that the following concentration and temperature dependency holds for each parameter:

$$P_j = A_j C^{B_j} \exp\left(-\frac{D_j}{T}\right), \tag{3}$$

where P_j, $j = 1, 2, \ldots, 6$, is the j-th model parameter ($P = \{G_0, k_0, \lambda, \varphi_\infty, \varphi_0, \vartheta\}$), while A_j, B_j and D_j are constant parameters, *i.e.*, the BMP model parameters have a van't Hoff-like relation with temperature and a power-law relation with concentration, respectively. For a first-order phase transition, the BMP model parameters (or at least some of them) should have an abrupt change with respect to temperature or concentration, while for a second-order phase transition the partial derivative of these parameters with respect to temperature or concentration should have an abrupt change. Thus, eq. (3) has different constant parameters (A_j, B_j and D_j) for each region of concentration or temperature where different phases exist or co-exist, and the specific points where these parameters change determine the phase transition boundaries. For simple shear, the equations that arise from the BMP model (eqs. (1)

and (2)) are

$$\frac{1}{G_0\varphi}\left(\frac{\mathrm{d}\sigma_{12}}{\mathrm{d}t}-\dot{\gamma}_{12}\sigma_{22}\right)+\sigma_{12}=\frac{\dot{\gamma}_{12}}{\varphi}\,, \tag{4}$$

$$\frac{1}{G_0\varphi}\frac{\mathrm{d}\sigma_{ii}}{\mathrm{d}t}+\sigma_{ii}=\Theta_{ii}, \tag{5}$$

$$\lambda\frac{\mathrm{d}\varphi}{\mathrm{d}t}+\varphi=\varphi_0+k_0\lambda\left(1+\vartheta\dot{\gamma}_{12}\right)\times\left(\varphi_\infty-\varphi\right)\sigma_{12}\dot{\gamma}_{12}. \tag{6}$$

In these equations, σ_{12} is the shear stress, $\dot{\gamma}_{12}$ is the shear rate, σ_{ii} ($i=1,2$, and 3) are the normal stresses, $\Theta_{ii}=\frac{2\dot{\gamma}_{12}\sigma_{12}}{G_0\varphi}$ for $i=1$, and $\Theta_{ii}=0$ for $i=2,3$, and ϑ is the shear banding intensity parameter, which is determined uniquely by the a EIT criterion, to set the stress plateau, that is similar to the Maxwell equal-area criterion to set the equilibrium pressure between vapor and liquid along an isotherm in the coexistence region. In fact, the value of the shear banding intensity parameter tends to zero at the flow region where the sigmoid in the stress *versus* shear rate plateau fades [17]. For steady state, eqs. (4) to (6) reduce to a cubic equation in terms of the shear rate and quadratic for the shear stress or the fluidity, *i.e.*,

$$\varphi_0\sigma_{12}-\dot{\gamma}_{12}+k_0\lambda\left(1+\vartheta\dot{\gamma}_{12}\right)\left(\varphi_\infty\sigma_{12}-\dot{\gamma}_{12}\right)\sigma_{12}\dot{\gamma}_{12}=0, \tag{7}$$

or

$$\left(\varphi_0-\varphi\right)\varphi+k_0\lambda\left(1+\vartheta\dot{\gamma}_{12}\right)\left(\varphi_\infty-\varphi\right)\dot{\gamma}_{12}^2=0. \tag{8}$$

The solution of either of these equations for the fluidity as a function of the shear stress is given by

$$2\hat{\varphi}=\varphi_0-k_0\lambda\left(1+\vartheta\dot{\gamma}_{12}\right)\dot{\gamma}_{12}^2 +\sqrt{\left[\varphi_0-k_0\lambda\left(1+\vartheta\dot{\gamma}_{12}\right)\dot{\gamma}_{12}^2\right]^2+4k_0\lambda\left(1+\vartheta\dot{\gamma}_{12}\right)\varphi_\infty\dot{\gamma}_{12}^2}, \tag{9}$$

where $\hat{\varphi}$ denotes the steady state fluidity, and the steady state shear and normal stresses are $\hat{\sigma}_{12}=\dot{\gamma}_{12}\hat{\varphi}$, $\sigma_{11}=2\hat{\sigma}_{12}^2/G_0$ and $\sigma_{22}=\sigma_{33}=0$, respectively.

In analogy with a gas-liquid phase transition, where the unstable or spinodal region appears whenever the condition $\mathrm{d}P/\mathrm{d}V<0$ is met (in plots of pressure *versus* molar volume plots for different isotherms [30]), the shear-induced unstable region appears when the conditions $\mathrm{d}\hat{\sigma}_{12}/\mathrm{d}\dot{\gamma}_{12}<0$ and null second derivative holds in shear stress *versus* shear rate plot for different isotherms [28]. The boundaries of the unstable region are computed by considering $\mathrm{d}\hat{\sigma}_{12}/\mathrm{d}\dot{\gamma}_{12}=0$ in eq. (7). Furthermore, the phase coexistence boundary can be calculated by setting the first derivative equal to zero together with the condition $\mathrm{d}^2\hat{\sigma}_{12}/\mathrm{d}\dot{\gamma}_{12}^2=0$. Finally, phase transitions with respect to temperature and concentration can be evaluated by considering $\mathrm{d}\hat{\sigma}_{12}/\mathrm{d}T=0$ and $\mathrm{d}\hat{\sigma}_{12}/\mathrm{d}C=0$, respectively.

3 Methodology

3.1 Experimental setup

Aqueous solutions in a range of 2 to 35 wt.% CTAT were prepared with deionized water and CTAT (> 98% pure from Sigma-Aldrich). The samples were made in glass bottles and subjected to ultrasound for an hour to be homogenized. Then they were placed in a water bath at 40 °C during two weeks under stirring for stabilization. Once the samples were completely homogeneous, they were kept for another week in the water bath at the measurement temperature (30 °C) to reach equilibrium. The rheological behavior of this system was studied in a TA instruments controlled stress rheometer AR-G2, with cone and plate geometry of 60 mm diameter and 1° angle for the solutions with moderate viscosity and 40 mm diameter and angle of 2° for the high viscosity solutions. The rheometer temperature was controlled at 30 °C during the measurements. In addition, a polarized light BX51 Olympus microscope operated at 30 °C was used to observe the structural behavior of the CTAT/water system at rest and under flow.

The rheological data of a 20 wt.% Pluronics P103 (from BASF) aqueous solution reported in [31], were used. These authors performed steady and oscillatory simple-shear experiments in a strain-controlled TA Instruments Ares-22 rheometer with a cone and plate geometry of 0.1 rad and 50 mm diameter, keeping constant concentration and variable temperature (from 30 to 42 °C).

3.2 Determination of phase transitions

The six BMP parameters $\{G_0, k_0, \lambda, \varphi_\infty, \varphi_0, \vartheta\}$ were obtained from independent experiments for each concentration and temperature. As explained elsewhere [29], G_0 and λ were determined from small-amplitude oscillatory shear, and φ_0 and φ_∞ were obtained from the fluidity *versus* shear rate flow curve. $k_0\lambda$ and ϑ were calculated by fitting eq. (7) to the shear stress *versus* shear rate data. Then, eq. (3) was used to estimate the correlation of each parameter as a function of temperature or concentration. If an abrupt change or a change in the slope of any parameter as a function of the temperature or surfactant concentration was detected, the fitting procedure was used to compute the precise point of the transition.

4 Results

4.1 CTAT/water system

The CTAT/water system is a good example of wormlike micellar solutions that exhibits flow-induced instabilities associated with changes in micellar conformations. In particular, CTAT is a cationic surfactant that forms wormlike micelles, even in the absence of any added inorganic or organic salt, at concentrations above 0.04 wt.% and 23 °C [32]. The length of these giant micelles depends on surfactant concentration, temperature and energy of micellar rupture [33]. This system may go through a transition between isotropic and nematic phases under an applied external stress [34].

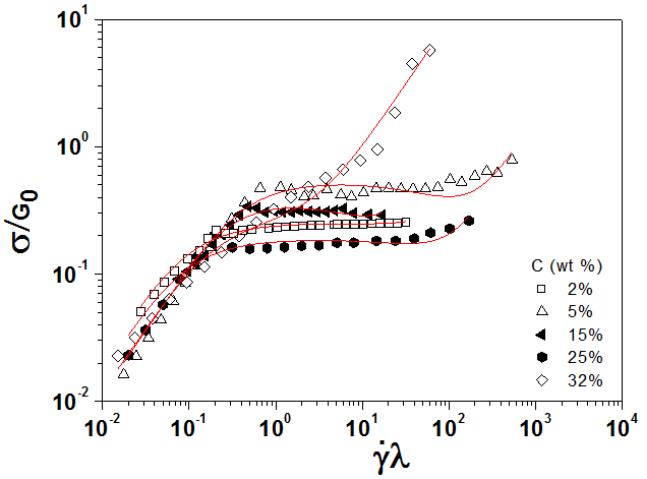

Fig. 1. Experimental data at steady state (symbols) and BMP model fits (continuous lines) for CTAT/water system at 30 °C for several CTAT concentrations.

Shear rate sweeps for the CTAT/water system at 2 to 35 wt.% were carried out. Figure 1 shows the master curves of normalized shear stress *versus* shear rate for selected CTAT concentrations. At low shear rates ($\dot{\gamma}\lambda <$ ca. 0.5), all samples follow a linear tendency with slope equal to 1 indicating that in this region the system behaves as a Newtonian fluid, followed by a shear thinning for concentrations smaller than 2 wt.% and larger than 31 wt.% or a stress plateau for concentrations between 2 and 31 wt.%, at $\dot{\gamma}\lambda =$ ca. 0.5. Past the shear-thinning region, all samples follow a linear tendency with slope equal to 1 (Newtonian flow) at high flow rates; however, for concentrations above 31 wt.%, the upper Newtonian branch appears at lower normalized shear rates. Notice that for concentrations larger than ca. 31 wt.%, the shear stress increases monotonically with respect to the applied shear stress, whereas from 2 to ca. 31 wt.%, for normalized shear rates from ca. 0.5 to 100, shear banding sets in at normalized stress plateau, σ/G_0, from 0.2 to 0.4.

Figure 2a shows a plot of the BMP parameters as a function of the surfactant concentration for the CTAT/water system. These parameters were computed as described in sect. 3.2. At ca. 31 wt.%, all parameters present an abrupt change (see fig. 2b that depicts a zoom of the concentration interval where the abrupt change was detected) indicating a first-order phase transition. Therefore, to adjust eq. (3), we define $\hat{A}_j = A_j \exp(-D_j/T)$ at constant temperature, and the concentration dependence has two regions before and after the transition with different parametric behavior:

$$P_j(C) = \begin{cases} \hat{A}_{1,j} C^{B_{1,j}}, & \text{if } C < 31, \\ D_j + E_j \dfrac{1 - \tanh(\frac{C-31.9}{0.05})}{2}, & \text{if } 31 \le C < 32, \\ \hat{A}_{2,j} C^{B_{2,j}}, & \text{if } C \ge 32, \end{cases}$$
$$\text{for } j = 1, 2, \ldots, 6, \qquad (10)$$

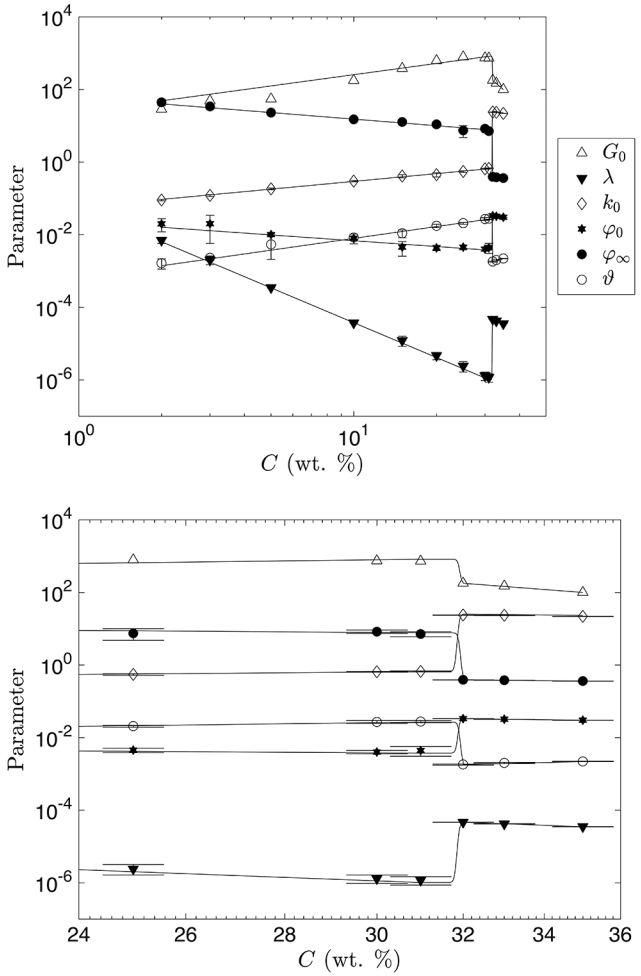

Fig. 2. Experimental and fits to eq. (10) of the BMP parameters for the CTAT/water system at 30 °C. (a) Full scale range. (b) Near the first-order transition.

where P_j is the j-th model parameter ($P = \{G_0, k_0, \lambda, \varphi_\infty, \varphi_0, \vartheta\}$) as a function of the surfactant concentration, C, and C_t is the phase transition concentration, both in wt.% surfactant. $\hat{A}_{i,j}$ and $B_{i,j}$ are the power-law constants for each BMP parameter, the values of which are reported in table 1, while $D_j = \hat{A}_{1,j} 31^{B_{1,j}}$ and $E_j = \hat{A}_{2,j} 32^{B_{2,j}} - \hat{A}_{1,j} 31^{B_{1,j}}$. Numerical computations reveal that the phase transition concentration occurs at $C_t = 31.9$ wt.%, since the abrupt change in the parameters was observed between 31 and 32 wt.% (see fig. 2). To calculate the derivatives of the stress with respect to C in the discontinuity we used a continuous approximation with a tangential expression for the abrupt change zone in the parameters, that was observed between 31 and 32 wt.%, which is an average expression between the two points (see the second line of eq. (10)). Notice that the functional form given in eq. (10) fits remarkably well the experimentally determined values of the model's parameters.

Figure 3 shows photographs of polarized light microscopy of the CTAT/water system. The photographs presented in figs. 3a and b were taken at rest for 30 and

Table 1. BMP model parameters for the CTAT/water system.

Parameter	G_0 (Pa)	λ (s)	k_0 (Pa)	φ_0 ($Pa^{-1}s^{-1}$)	φ_∞ ($Pa^{-1}s^{-1}$)	ϑ (s)
$\hat{A}_{1,j}$	23.8	0.057	0.058	0.023	60.8	6.56×10^{-4}
$\hat{A}_{2,j}$	1.16×10^{12}	738	2.38	1.73	8.7	1.43×10^{-6}
$B_{1,j}$	1.03	0.711	−3.19	−0.53	−0.602	1.08
$B_{2,j}$	−6.52	−0.99	−3.13	−1.14	−0.895	2.06

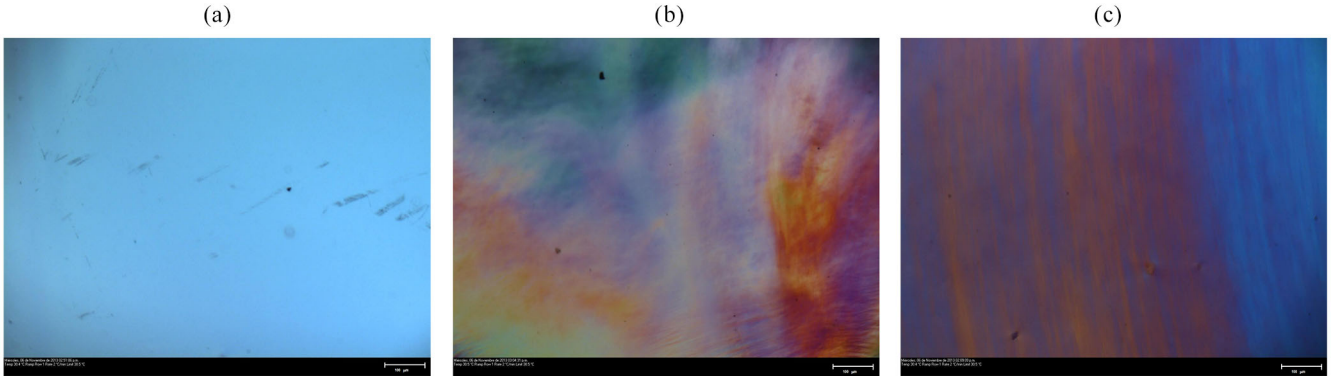

Fig. 3. Polarized light photomicrographs of CTAT/water system at 30 °C. (a) Isotropic phase at rest (without shear) for 30 wt.%. (b) Nematic phase at rest (without shear) for ca. 32 wt.%. (c) Nematic phase under a shear rate of $10\,s^{-1}$ for ca. 32 wt.%.

32 wt.% samples, respectively, while the photograph in fig. 3c shows the structure of the 32 wt.% CTAT sample examined at a shear rate of $10\,s^{-1}$. A polarizing optical microscopy (POM) texture, which is absent in fig. 3a, is indicative of an isotropic phase, whereas the photographs in figs. 3b and c show POM textures that are characteristic of a nematic phase [35]. When shear is applied to the nematic phase, the intensity of the POM texture is larger, indicating a restructuring of the system (fig. 3c). The BMP parameters present an abrupt change between 31 and 32 wt.%, and the POM texture of the phase transition are in concordance with results of Pal *et al.* [34], who reported a phase transition for a quiescent CTAT/water solution at 32 wt.% content and 30 °C.

Figure 4 depicts the concentration *versus* shear rate phase diagram for the CTAT/water system at 30 °C considering the shear rates at which $d\hat{\sigma}_{12}/d\dot{\gamma}_{12} = 0$ (continuous lines), $d^2\hat{\sigma}_{12}/d\dot{\gamma}_{12}^2 = 0$ (dashed line), $d\hat{\sigma}_{12}/dC = 0$ (dotted lines) and $d^2\hat{\sigma}_{12}/dC^2 = 0$ (dash-dotted line) hold, as described in sect. 2. In particular, the shear rates and concentrations at which $d\hat{\sigma}_{12}/d\dot{\gamma}_{12} = 0$ enclose the instability region (dark gray region) where shear banding appears, while the shear rates and concentrations at which $d\hat{\sigma}_{12}/dC = 0$ contains the nematic-isotropic coexistence region (light gray region) that is around 31 to 32 wt.%, with a concentration range that decreases as shear rate increases (see the insert in fig. 4). This diagram clearly depicts the effect of dissipative flows in the change of structures, phase transitions and instability in micellar systems. As described above, to construct fig. 4, we used eq. (10) with $C_t = 31.9$ wt.%. Thus, for concentrations below 31.9 wt.%, we used the set of parameters $\hat{A}_{1,j}$ and $B_{1,j}$, while for concentration above 31.9 wt.% we used the set of parameters $\hat{A}_{2,j}$ and $B_{2,j}$, reported in table 1 (fig. 2b shows the continuous parameters variation used to compute fig. 4). Notice that although an abrupt change in the parameters exists, the variation of the instability region is continuous. At low concentrations, the effect of the shear rate is practically negligible on the structural configuration of the system, because predominant short cylindrical structures are present; in particular, for concentrations below ca. 3.7 wt.% the system presents shear thinning with an inflection point shown in fig. 4 with the dashed line ($d^2\hat{\sigma}_{12}/d\dot{\gamma}_{12}^2 = 0$). Notice in the insert of fig. 4 that the shear rate at which this inflection occurs increases as concentration increases. As the concentration increases at rest or at relatively low shear rates, a wormlike micellar structure is formed together with isotropic-phase aggregations, but above around 28 wt.% [32] to 33 wt.% [34], it has been reported that a nematic phase, N_1, appears, while according to our calculations, this phase transition takes place around 31 to 32 wt.% (an estimation of this phase transition is depicted in fig. 4 with the dotted lines), where the nematic-isotopic coexistence region ($I + N_1$) appears. At shear rates larger than $300\,s^{-1}$, the structure is completely destroyed and a nematic phase of short cylindrical micelles (N_2) are present at all concentrations. We believe that the micellar solution with isotropic

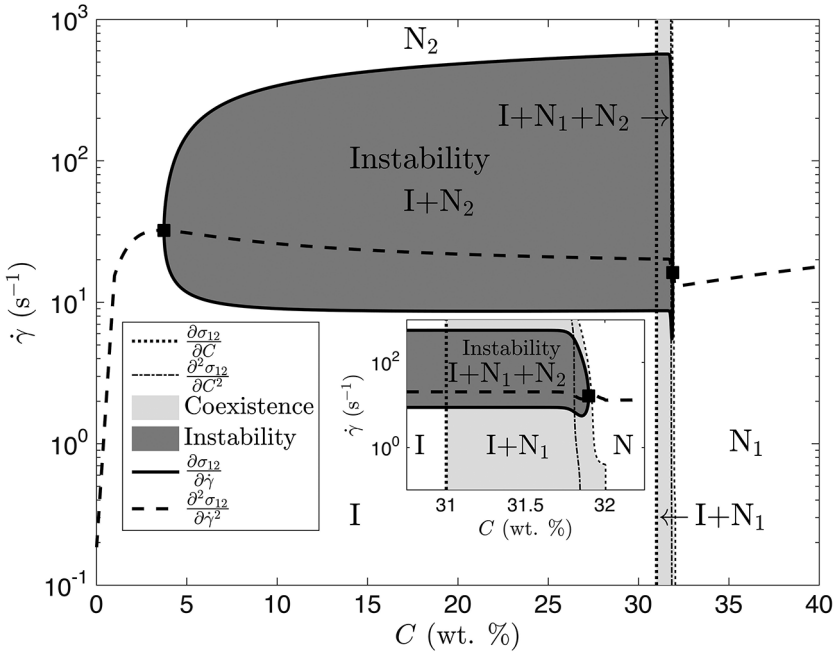

Fig. 4. Phase plane of shear rate *versus* concentration for CTAT/water at 30 °C.

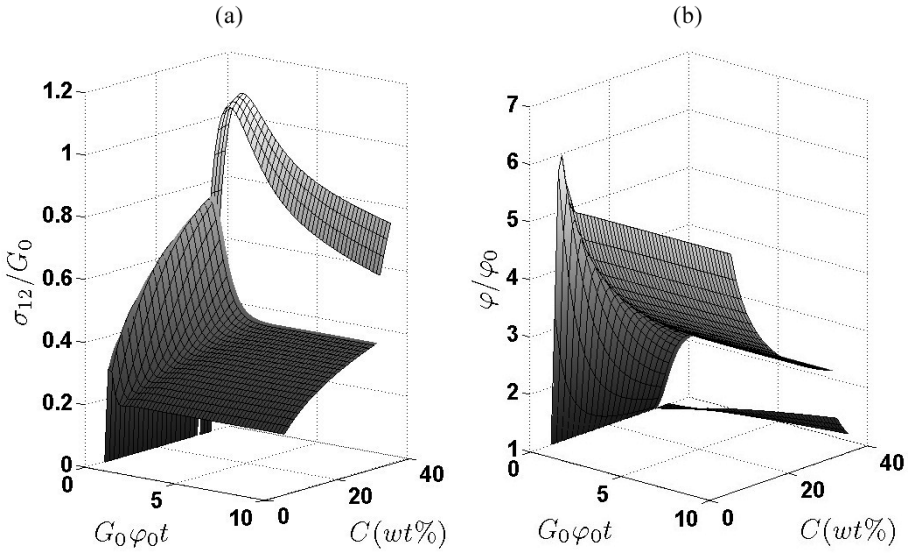

Fig. 5. Transient response of the CTAT/water system at 30 °C as a function of concentration. (a) Shear stress. (b) Fluidity.

wormlike micelles, I, under the effect of high shear rates are destroyed and giant wormlike micelles begin separating gradually into smaller micelles until they are short cylindrical micelles in a nematic phase induced by shear. The boundary given by the dashed line at low concentrations is the inflection point and represents a gradual transition between isotropic wormlike micelles, I, and nematic phase of short cylindrical micelles, N_2, that could be reached at low concentrations and/or high shear rates, where isotropic wormlike micelles structures, I, are completely destroyed and the nematic phase of short cylindrical micelles (N_2) is present at all concentrations with bigger or smaller proportion. At shear rates and concentrations between 10 and 300 s^{-1} and between approximately 3.7 and 32 wt.%, an unstable two-phase region, with coexistence of isotropic wormlike micelles, I, and nematic phase of short cylindrical micelles, N_2, induces shear banding flow. The coexistence points (solid squares in fig. 4), where both $d\hat{\sigma}_{12}/d\dot{\gamma}_{12}$ and $d^2\hat{\sigma}_{12}/d\dot{\gamma}_{12}^2$ are equal to zero, appear at approximately 3.7 wt.% and 32 wt.% and shear rates of 32 and 16 s^{-1}, respectively. Inside the instability region (with concentrations around 31 and 32 wt.%) it is possible to have isotropic wormlike micelles, nematic phase of short cylindrical micelles and nematic structures

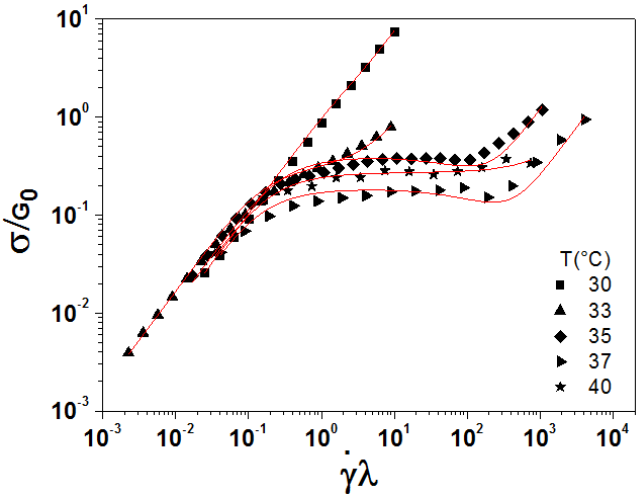

Fig. 6. Experimental data at steady state (markers) and BMP model fits (continuous lines) for 20 wt.% Pluronics P103/water system at several temperatures.

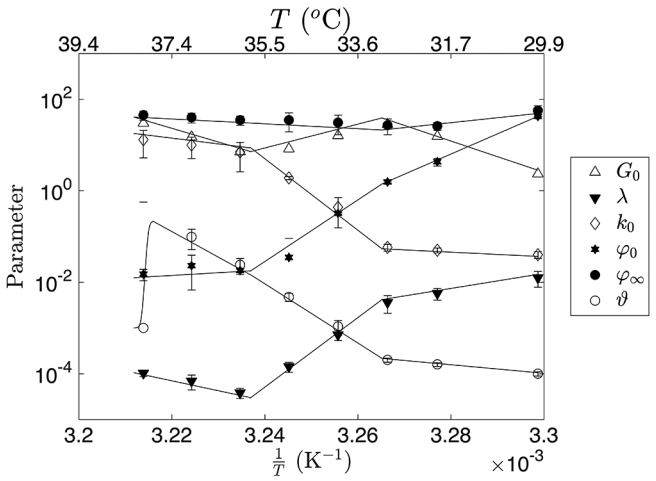

Fig. 7. Experimental values of the BMP parameters for the 20 wt.% Pluronic P103/water system. Zone I: spherical micellar phase, zone II: cylindrical micellar phase, and zone III: nematic phase.

that produce shear banding, in agreement with the experimental results shown in fig. 3c.

The transient behavior as a function of shear rate of the CTAT/water system for several concentrations in the region of shear banding flow ($\dot{\gamma}\lambda = 1$) is presented in fig. 5. In particular, fig. 5a and b show the evolution of shear stress and fluidity. The system presents an initial overshoot in the shear stress at all concentrations. However, the overshoot magnitude increases as the concentration increases. Remarkably, around 31 to 32 wt.%, the transient behavior changes considerably due to a phase transition. A sudden enhancement in the overshoot is observed at this concentration, which evolves into an unstable flow behavior.

4.2 Pluronics P103/water system

Pluronics^{TM} are triblock copolymers of polyethylene oxide (PEO) and polypropylene oxide (PPO), PEO-PPO-PEO. These systems have interesting amphiphilic properties showing self-assembly in aqueous solutions. Particularly, the Pluronics P103/water system has the ability to form spherical micelles at concentrations above the cmc; as the Pluronics concentration is increased, cylindrical or lamellar structure form, and when the concentration is raised further, a phase transition to liquid crystals occurs [36]. The experimental data of shear rate sweeps for the 20 wt.% Pluronics P103 at temperatures between 30 and 42 °C were reported in [31].

Figure 6 shows the normalized shear stress *versus* shear rate master curves for some of these temperatures. For normalized shear rates smaller than 0.5, all data collapse into a straight line with slope equal to 1, indicating a Newtonian behavior. At low temperatures the system has a Newtonian behavior practically for every shear rate; however, approximately at 33 °C the system begins to exhibit shear thinning behavior, and approximately from 34 to 37 °C, the system has a plateau region where a transition in the micellar phase structures occurs, and shear banding flow is detected. Above 37 °C, the sigmoidal behavior disappears but the system still exhibits shear thinning.

Figure 7 presents a plot of the BMP parameters as a function of temperature for a 20 wt.% Pluronics P103 aqueous solution. These parameters were computed as described in sect. 3.2. In contrast to the previous systems, the parameters do not exhibit discontinuities but a continuous behavior with changes in slope at the structural transitions. In fact, between 33 and 34 °C, the curves for G_0, k_0, λ, ϑ and φ_∞ and between 35 and 36 °C the curves for G_0, k_0, λ and φ_0 exhibit a change in their slope, indicating second-order phase transitions. To adjust eq. (3), we define $\bar{A}_j = A_j C^{B_j}$ and, according with the slope changes in fig. 7, three regions of temperature dependence were identified, where each of these three regions corresponds to the structures shown in the experimental phases diagram of Álvarez-Ramírez *et al.* [37]. Since the rheological measurements were made at constant P103 concentration, the temperature behavior in the three regions can be expressed as

$$P_j(T) = \begin{cases} \bar{A}_{1,j} e^{-D_{1,j}/T}, & \text{if } T < T_1, \\ \bar{A}_{2,j} e^{-D_{2,j}/T}, & \text{if } T_1 \le T < T_2\,, \quad \text{for } j = 1, 2, \ldots, 6, \\ \bar{A}_{3,j} e^{-D_{3,j}/T}, & \text{if } T \ge T_2, \end{cases} \tag{11}$$

where P_j is the j-th model parameter ($P = \{G_0, k_0, \lambda, \varphi_\infty, \varphi_0, \vartheta\}$) as a function of temperature, T, in degrees Kelvin. $\bar{A}_{i,j}$ and $D_{i,j}$ are the coefficients of the van't Hoff-like equation for each parameter, whereas T_1 and T_2 represent the temperature at which the transitions occur. To

Table 2. BMP model parameters for the P103/water system.

Parameter	G_0 (Pa)	λ (s)	k_0 (Pa)	φ_0 ($\mathrm{Pa^{-1}s^{-1}}$)	φ_∞ ($\mathrm{Pa^{-1}s^{-1}}$)	ϑ (s)
$\ln \bar{A}_{1,j}$	260	34.3	−129	−331	−78.2	61.6
$\ln \bar{A}_{2,j}$	−192	585	−577	−506	43.5	478
$\ln \bar{A}_{3,j}$	225	96.0	151	−48.8	42.4	413
$D_{1,j}$	7.86×10^4	1.14×10^4	-3.78×10^4	-1.02×10^5	-2.49×10^4	2.15×10^4
$D_{2,j}$	-6.00×10^4	1.80×10^5	-1.75×10^5	-1.55×10^5	1.24×10^4	1.49×10^5
$D_{3,j}$	6.90×10^4	2.90×10^4	5.00×10^4	-1.38×10^4	1.2×10^4	1.29×10^5

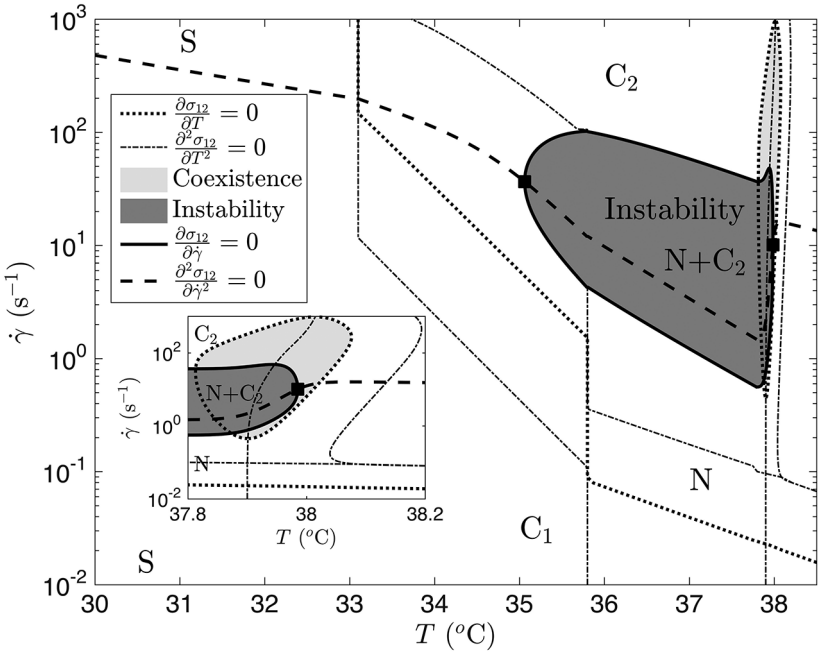

Fig. 8. Phase plane of the shear rate *versus* concentration for the Pluronics P103/water system at 20 wt.%.

identify these temperatures, in addition to $\bar{A}_{i,j}$ and $D_{i,j}$ (see table 2), T_1 and T_2 were estimated with the fitting procedure, obtaining $T_1 = 33.1\,^\circ$C and $T_2 = 35.8\,^\circ$C. Notice that the van't Hoff functional relation fits the data very well below and above the phase transition. The model parameters for this system are smooth functions of temperature only with changes in their slopes, therefore the partial derivative can be straightforward computed without any approximation, except for the parameter ϑ that presented a abrupt change near the cloud point (at around 38 °C) as shown in fig. 7.

Figure 8 shows the out-of-equilibrium phase diagram of shear rate *versus* temperature for the 20 wt.% P103/water solution. As in the phase diagram of the CTAT/water system (fig. 4), the continuous, dashed, dotted and dashed-dotted lines in fig. 8 represent the points where $\mathrm{d}\hat{\sigma}_{12}/\mathrm{d}\dot{\gamma}_{12} = 0$, $\mathrm{d}^2\hat{\sigma}_{12}/\mathrm{d}\dot{\gamma}_{12}^2 = 0$ $\mathrm{d}\hat{\sigma}_{12}/\mathrm{d}T = 0$ and $\mathrm{d}^2\hat{\sigma}_{12}/\mathrm{d}T^2 = 0$ hold, respectively. The dark gray region, enclosed by the continuous lines, shows an instability region, while the light gray region, enclosed by the dotted region, shows a coexistence region. In this system, a spherical micellar phase (S) appears at low temperatures and low and high shear rates with a slight shear thinning at high shear rates due to the self-association of these spherical structures to form cylindrical micelles (see the dashed line at temperature below 33 °C). Then, the spherical micellar phase is followed by cylindrical structures (C_1) that form at temperatures around 33 and 36 °C at low shear rates. In this temperature range, as the shear rate increases, the cylindrical structures align producing a gradual transition, that takes place at lower temperatures (the dotted and dotted-dashed lines represent an estimation of this transition) as the shear rate increases. At higher shear rates, shear thinning appears (the dashed line at temperature between 33 and 35 °C) indicating a gradual disruption of the cylindrical structures (C_1), producing smaller

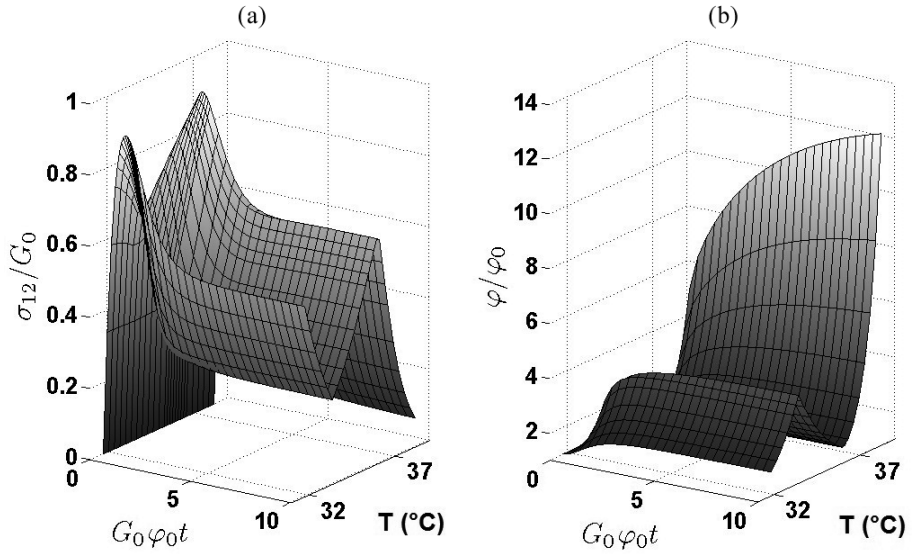

Fig. 9. Transient response for Pluronics P103/water system at 20 wt.% as a function of temperature. (a) Shear stress. (b) Fluidity.

cylindrical structures (C_2). We believe that under high shear rates due to high shear stress cylindrical structure can be destroyed and produces smaller cylindrical structures. At low shear rates and around 36 °C, a transition occurs where cylindrical micelles are reorganized in a nematic phase (N), induced by the shear.This is consistent with the calculations shown in fig. 8, where $\mathrm{d}\hat{\sigma}_{12}/\mathrm{d}T = 0$ and/or $\mathrm{d}^2\hat{\sigma}_{12}/\mathrm{d}T^2 = 0$, indicating maximum and/or inflection points of the shear rate with respect to temperature due to this transition. Between approximately 35 and 38 °C and at high shear rates, a region of instability with coexistence between cylindrical micelles and a cylindrical nematic phase induced by shear is observed (N + C_2), where shear banding flow develops. At higher temperatures and higher shear rates, a disruption of the flow-induced structures occurs. According to the behavior of the BMP parameters with temperature, the first transition detected at 33.1 °C corresponds to the point where the transition between the spherical micellar phase and the cylindrical structures occurs at high shear rates, in agreement with the variation in the slope of the shear banding intensity parameter, ϑ (see fig. 7). The second transition, detected at 35.8 °C represents the transition between the cylindrical and the nematic phase. Finally, in contrast with the previous two transitions, where only the slopes of the parameters change, the third transition occurs around 38 °C, where the instability region disappears and a region of coexistence sets in (light gray color enclosed by the dotted lines), consistent with the cloud-point temperature reported by Álvarez-Ramírez *et al.* [37]. In the BMP model, this transition is correlated with an abrupt change in the shear banding intensity parameter, ϑ, shown in fig. 7.

Figure 9 shows the transient behavior of the P103/water systems as a function of temperature and shear rate in the region of shear banding flow ($\dot{\gamma}\lambda = 10$). The shear stress (fig. 9a) and the fluidity (fig. 9b) present a minimum and a maximum in the temperature axis, respectively. This system also presents an initial overshoot in the shear stress whose maximum varies with respect to temperature, while the time response is similar in the full range of temperatures.

5 Conclusions

The existence and classification of transition points in micellar systems can be predicted by analyzing the behavior of the BMP parameters upon fitting the rheological data. The proposed methodology is general and can be applied to micellar systems exhibiting shear-induced phase transitions. In particular, this methodology was applied to two widely different micellar systems. For the CTAT/water system, a thermodynamic first-order phase transition induced by flow is due to the change in the external structural rearrangement of elongated wormlike micelles, where the internal energy in the system is not modified. For this case, the parameters of the BMP model, fitted to the rheological data *versus* concentration, exhibit an abrupt change at the phase transition. For the P103/water system, the out-of-equilibrium second-order structural-thermodynamic transitions are due to the change in the structural conformation of micelles, involving a change in the internal energy induced by increasing temperature in the rheological experiments. Here, the parameters of the BMP model, fitted to the experimental data, exhibit a change in slope as a function of temperature, not an abrupt change, where these structural (not phase) transitions occur, while the abrupt change of the shear banding intensity parameter around 38 °C represents a thermodynamic first-order phase transition correlated with phase separation (cloud point).

We acknowledge support from CONACYT, The National Science and Technology Council through the research grant No. 269328.

Author contribution statement

All authors contributed equally to the paper.

References

1. S.M. Fielding, P.D. Olmsted, Eur. Phys. J. E **11**, 65 (2003).
2. M. Cates, Macromolecules **20**, 2289 (1987).
3. J.E. Puig, F. Bautista, J.F.A. Soltero, O. Manero, *Giant Micelles: Properties and Applications: Surfactant Science Series*, edited by Raoul Zana, Eric W. Kaler (CRC Press, 2007).
4. G. Porte, J.F. Berret, J.L. Harden, J. Phys. II **7**, 459 (1997).
5. J.F. Berret, D.C. Roux, G. Porte, J. Phys. II **4**, 1261 (1994).
6. F. Bautista, J. Soltero, J. Pérez-López, J. Puig, O. Manero, J. Non-Newton. Fluid Mech. **94**, 57 (2000).
7. C. Grand, J. Arrault, M. Cates, J. Phys. II **7**, 1071 (1997).
8. S. Lerouge, J. Decruppe, C. Humbert, Phys. Rev. Lett. **81**, 5457 (1998).
9. C.Y.D. Lu, P.D. Olmsted, R. Ball, Phys. Rev. Lett. **84**, 642 (2000).
10. R. Mair, P. Callaghan, Europhys. Lett. **36**, 719 (1996).
11. R. Miller, *Giant Micelles: Properties and Applications: Surfactant Science Series*, edited by Raoul Zana, Eric W. Kaler (CRC Press, 2007).
12. D.C.H. Rehage, H. Hoffmann, *Shear Induced Phase Transitions in Highly Dilute Aqueous Detergent Solutions* (Springer, 1982).
13. J.B Salmon, A. Colin, S. Manneville, F. Molino, Phys. Rev. Lett. **90**, 228303 (2003).
14. N. Spenley, M. Cates, T. McLeish, Phys. Rev. Lett. **71**, 939 (1993).
15. S. Hess, P. Ilg, Rheol. Acta. **44**, 465 (2005).
16. S. Hess, Z. Naturforsch. A **30**, 728 (1975).
17. F. Bautista, J. Soltero, E. Macias, J. Puig, O. Manero, J. Phys. Chem. B **106**, 13018 (2002).
18. E. Macías, F. Bautista, J. Soltero, J. Puig, P. Attane, O. Manero, J. Rheol. **47**, 643 (2003).
19. G. Landázuri, E.R. Macías, J.P. García-Sandoval, E. Hernández, O. Manero, J.E. Puig *et al.*, Rheol. Acta. **55**, 547 (2016).
20. J. Escalante, E. Macias, F. Bautista, J. Pérez-López, J. Soltero, J. Puig *et al.*, Langmuir **19**, 6620 (2003).
21. O. Manero, J. Pérez-López, J. Escalante, J. Puig, F. Bautista, J. Non-Newton. Fluid Mech. **146**, 22 (2007).
22. O. Manero, F. Bautista, J. Soltero, J. Puig, J. Non-Newton. Fluid Mech. **106**, 1 (2002).
23. T. McLeish, R. Larson, J. Rheol. **42**, 81 (1998).
24. E. Boek, J. Padding, V. Anderson, P. Tardy, J. Crawshaw, J. Pearson, J. Non-Newton. Fluid Mech. **126**, 39 (2005).
25. M.J. Armstrong, A.N. Beris, S.A. Rogers, N.J. Wagner, J. Rheol. **60**, 433 (2016).
26. P.E. Martínez, *Termodinámica básica y aplicada* (Dorssat, 1984).
27. H.B. Callen, *Thermodynamics and an Introduction to Thermostatistics* (John Wiley & Sons, 2006).
28. F. Bautista, J. Pérez-López, J. García, J. Puig, O. Manero, J. Non-Newton. Fluid Mech. **144**, 160 (2007).
29. F. Bautista, V. Fernández, E. Macı, J. Pérez-López, J. Escalante, J. Puig *et al.*, J. Non-Newton. Fluid Mech. **177**, 89 (2012).
30. S.I. Sandler *et al.*, *Chemical, Biochemical, and Engineering Thermodynamics*, Vol. **4** (John Wiley & Sons, Hoboken, 2006).
31. V. Fernández, N. Tepale, J. Alvarez, J. Pérez-López, E. Macı, F. Bautista *et al.*, J. Colloid Interface Sci. **336**, 842 (2009).
32. J. Soltero, J. Puig, O. Manero, P. Schulz, Langmuir **11**, 3337 (1995).
33. R.G. Larson, *The Structure and Rheology of Complex Fluids*, Vol. **33** (Oxford University Press, New York, 1999).
34. A. Pal, R. Mary, V. Raghunathan, J. Mol. Liq. **174**, 48 (2012).
35. D. Guillon, P. Cladis, J. Stamatoff, Phys. Rev. Lett. **41**, 1598 (1978).
36. G. Riess, Prog. Polym. Sci. **28**, 1107 (2003).
37. J. Álvarez-Ramírez, V. Fernández, E. Macías, Y. Rharbi, P. Taboada, R. Gámez-Corrales *et al.*, J. Colloid Interface Sci. **333**, 655 (2009).